Relationship between Thermodynamics and Mechanism during Photoinduced Charge Separation in Reaction Centers from *Rhodobacter sphaeroides*†

Neal W. Woodbury,* Jeffrey M. Peloquin, Rhett G. Alden,‡ Xiaomei Lin, Su Lin, Aileen K. W. Taguchi, JoAnn C. Williams, and James P. Allen

Department of Chemistry and Biochemistry and the Center for the Study of Early Events in Photosynthesis, Arizona State University, Tempe, Arizona 85287-1604

Received January 27, 1994; Revised Manuscript Received April 19, 1994®

ABSTRACT: Detailed fast transient absorption measurements have been performed at low temperature on reaction centers from *Rhodobacter sphaeroides* strain R-26 and on a double mutant, [LH(L131)+LH-(M160)], in which the P/P^+ oxidation potential is roughly 140 mV (1100 cm^{-1}) above that of wild-type reaction centers. In both samples, the decay of the excited singlet state of the initial electron donor is not well described by a single-exponential decay term. This is particularly true for reaction centers from the double mutant where at least three exponential kinetic components are required to describe the decay, with time constants ranging from a few picoseconds to hundreds of picoseconds. However, singular value decomposition analysis of the time-dependent absorption change spectra indicates the presence of only two spectrally distinct states in reaction centers from both R-26 and the double mutant. Thus, the complex decay of P* at low temperature does not appear to be due to formation of either the state $P^+B_A^-$ as a distinct intermediate in electron transfer or $P^+B_B^-$ as an equilibrated side product of electron transfer. Instead, the decay kinetics are modeled by assuming dynamic solvation of the charge-separated state, as was done for the long-lived fluorescence decay in the accompanying paper [Peloquin, J. M., Williams, J. C., Lin, X., Alden, R. G., Taguchi, A. K. W., Allen, J. P., & Woodbury, N. W. (1994) *Biochemistry 33*, 8089–8100]. The results of assuming a static distribution of electron-transfer rates at early times followed by dynamic solvation of the charge-separated states on longer time scales are also presented. Regardless of which model is used to describe the early time kinetics of excited-state decay, the time-dependent excited-state population on the 100-ps or longer time scale is best described in terms of thermal repopulation of P* from the charge-separated state, even at 20 K. This results in a time- and temperature-dependent driving force estimated for initial electron transfer of less than 200 cm^{-1} on all time scales from picoseconds to nanoseconds. Assuming a nonzero internal reorganization energy associated with charge separation, the small driving force does not appear to be consistent with the lack of temperature dependence of electron transfer and the fact that a mutant with a P/P^+ oxidation potential 140 mV (1100 cm^{-1}) higher than wild type is still able to undergo electron transfer, even at low temperature. These observations are more in line with an essentially adiabatic electron-transfer reaction near the strong coupling limit.

The initial photosynthetic electron-transfer reactions of purple nonsulfur bacteria are carried out by the reaction center, a protein–cofactor complex embedded in the photosynthetic membrane. The structure of this complex has been determined by X-ray crystallography in two species (Deisenhofer et al., 1984; Allen et al., 1987; Chang et al., 1991), and the electron-transfer pathway has been studied extensively by various spectroscopic techniques [for reviews, see Kirmaier and Holten (1987), Feher et al. (1989), and Parson (1991)]. The present understanding of photosynthetic electron transfer is that light energy absorbed by antenna complexes or reaction center cofactors is transferred to a dimer of bacteriochlorophylls (P)[1] on the periplasmic side of the reaction center, forming P*, the excited singlet state of P. The mechanism of the electron-transfer reaction that follows is still unclear, but within 3.5 ps a charge-separated state is formed that involves the cation of P (P^+) and the anion of a bacteriopheophytin (H_A^-). The electron is subsequently transferred to a quinone on the 200-ps time scale.

Much of the confusion concerning the initial electron-transfer reaction stems from the observation that the kinetics of P* decay and charge separation are not accurately described by a single-exponential decay term as one would expect for a simple first-order reaction (Holzapfel et al., 1989, 1990; Vos et al., 1991, 1992; Du et al., 1992; Muller et al., 1992; Hamm et al., 1993). In addition, the rate constant associated with the formation of the charge-separated state is wavelength dependent, at least at some temperatures (Kirmaier & Holten, 1990, 1991). In the structure of the photosynthetic reaction center from either *Rhodopseudomonas viridis* or *Rhodobacter sphaeroides*, there are several cofactors in the vicinity of the special pair in addition to H_A. A monomer bacteriochlorophyll

† This work was supported by Grants DMB91-58251 and MCB 9219378 from the National Science Foundation, Grants GM41300 and GM45902 from the National Institutes of Health, and a Postdoctoral Fellowship in Plant Biology, DIR-9104322, from the NSF. Instrumentation was purchased with funds from NSF Grant DIR-8804992 and Department of Energy Grants DE-FG-05-88-ER75443 and DE-FG-05-87-ER75361. This is publication No. 201 from the Arizona State University Center for the Study of Early Events in Photosynthesis. The Center is funded by DOE Grant DE-FG-88-ER13969 as a part of the USDA/DOE/NSF Plant Science Centers Program.

* Corresponding author.

‡ Present address: Department of Biochemistry, SJ-70, University of Washington, Seattle, WA 98195.

® Abstract published in *Advance ACS Abstracts,* June 1, 1994.

[1] Abbreviations: P, bacteriochlorophyll dimer; B, bacteriochlorophyll monomer; H, bacteriopheophytin monomer; EDTA, ethylenediaminetetraacetic acid; Tris, tris(hydroxymethyl)aminomethane; ns, nanosecond; ps, picosecond; fs, femtosecond; *Rps.*, *Rhodopseudomonas*; *Rb.*, *Rhodobacter*.

0006-2960/94/0433-8101$04.50/0

molecule (B_A) is situated roughly between P and H_A. Two other chromophores, another monomer bacteriochlorophyll (B_B) and another bacteriopheophytin (H_B), are near P in positions approximately related to the positions of B_A and H_A by a C_2 axis of symmetry (Deisenhofer et al., 1984; Allen et al., 1987; Chang et al., 1991). One possible explanation for the complex kinetics observed at early times is that additional excited or charge-separated states are involved. Holzapfel et al. (1989) have suggested that the initial electron-transfer reaction involves the formation of $P^+B_A^-$ as an intermediate electronic state between P* and $P^+H_A^-$. It is also possible that $P^+B_B^-$ and/or $P^+H_B^-$ could serve as parallel products of P* decay [Hamm et al., 1993; also discussed by Muller et al. (1992)].

However, these models do not easily explain the large number of kinetic components which have been observed over many time scales in reaction center fluorescence decay and absorption change measurements. P* decay has been shown to involve kinetic components on the 1–4-ps time scale, the 10-ps time scale, the 100-ps time scale, and, in reaction centers where transfer to the quinone is blocked, the nanosecond time scale (Sebban & Moya, 1983; Woodbury & Parson, 1984; Kirmaier & Holten, 1993; Vos et al., 1991; Du et al., 1992; Williams et al., 1992a; Muller et al., 1992; Hamm et al., 1993; Peloquin et al., 1994). In addition, a significant wavelength dependence of the kinetics of both the first and the second electron-transfer reaction has been observed on the 1–4-ps and 100–200-ps time scales, respectively (Kirmaier et al., 1985; Kirmaier & Holten, 1987, 1990). Since it is unlikely that distinct electronic intermediates are present on all of these time scales, much of the complexity has been attributed to reaction center conformational heterogeneity that is either static (Kirmaier & Holten, 1990; Du et al., 1992; Muller et al., 1992) or dynamic [Kirmaier et al., 1985; Woodbury & Parson, 1984; also discussed in Muller et al. (1992)].

In the preceding paper in this issue (Peloquin et al., 1994), results were presented from fluorescence decay measurements performed on the 10-ps to 10-ns time scale using reaction centers from *Rb. sphaeroides* strain R-26 and two mutants, LH(L131) and the double mutant [LH(L131)+LH(M160)], that introduce hydrogen bonds between the protein and P (Williams et al., 1992a,b). These two mutations result in increases of 80 mV (650 cm^{-1}) and 140 mV (1100 cm^{-1}), respectively, in the P/P^+ oxidation potential. It was shown that much, if not all, of the long-lived fluorescence from reaction centers could be assigned to thermal repopulation of the excited singlet state of P from the charge-separated state, and that the fluorescence due to thermal repopulation of P* persisted at temperatures as low as 20 K, especially in the high-potential mutants. The fluorescence was analyzed in terms of a dynamic solvation model similar to models previously developed (Woodbury & Parson, 1984; Goldstein et al., 1988). In the dynamic solvation model, the free energy of the charge-separated state decreases as a function of time after electron transfer, resulting in a nonexponentially decreasing fluorescence level due to thermal repopulation of P*. Since the fluorescence persists at low temperature, this model predicts a very small free energy change for the P* to $P^+H_A^-$ reaction at 20 K even on the nanosecond time scale [less than 200 cm^{-1} for R-26 reaction centers and less than 100 cm^{-1} for the high-potential mutants; see the accompanying paper (Peloquin et al., 1994)]. Even lower free energy gaps were estimated for this reaction on the tens of picosecond time scale.

In this report, we extend the investigation of the complex P* decay kinetics in reaction centers by analyzing transient absorption data on the picosecond time scale, which is more relevant to the initial electron-transfer reaction itself. Preliminary room temperature measurements of femtosecond transient absorption changes associated with electron transfer in the double mutant indicated that the decay of P* was slower than that in wild type (25 vs 3.5 ps; Williams et al., 1992b). In the accompanying paper, it is shown that the amount of the 10-ps to 1-ns fluorescence in both R-26 reaction centers (which have a P/P^+ potential essentially identical to that of wild type) and the double hydrogen bond mutant increases significantly at low temperature compared to that observed at room temperature (Peloquin et al., 1994). In the case of the double hydrogen bond mutant, the increase is sufficient to make the equilibrium population of P* visible in transient absorption measurements for hundreds of picoseconds after excitation. In order to further investigate the mechanism underlying the P* decay time course at 20 K, a detailed study of the ultrafast transient absorption changes was performed at this temperature on reaction centers from both the carotenoidless strain R-26 and the double hydrogen bond mutant [LH(L131)+LH(M160)].

MATERIALS AND METHODS

Bacterial Strains and Reaction Center Isolation. Bacterial growth and reaction center isolation were performed as described in Peloquin et al. (1994).

Femtosecond-Resolution Pulse–Probe Transient Absorption Spectroscopy. The pulse–probe transient absorption apparatus has been described previously (Taguchi et al., 1992). It was modified for this work with the addition of a continuum reamplification stage. The roughly 200-μJ, 590-nm, 200-fs pulse which emerges from the 540-Hz pulsed-dye amplifier was split into two equal parts. Each half of the beam was used to generate a continuum. One of these continuum pulses was split again and used as the sample and reference probe beams as described previously (Taguchi et al., 1992). The other half was sent through an 880-nm interference filter with a spectral band width (full width at half-maximum) of 10 nm and reamplified in a prism amplifier stage (Santa Ana Lasers) pumped with about 2 mJ of 532-nm light from the 540-Hz regenerative Nd:YAG amplifier (Continuum). The dye used for reamplification was LDS867 (Exciton) in a roughly 10:1 (v/v) mixture of ethylene glycol and propylene carbonate. The resulting roughly 10-μJ pulses were passed through a polarizer and a half-wave plate to define the polarization and then focused to a 1–2-mm-diameter spot on the sample. The final excitation pulse energy at the sample was roughly 5 μJ. For all experiments reported, the relative polarization of the pulse and probe beams was at the magic angle. The total fraction of the reaction centers in the sample which absorbed a photon was 0.15–0.20.

All measurements reported were performed at a temperature of 20 K using a helium displex as described by Williams et al. (1992a). The sample concentrations were adjusted to give an optical density at 800 nm of 1.6–1.8 at the temperature of the measurement. The sample was prepared in 67% (v/v) glycerol, 50 mM Tris-HCl (pH 8.0), 0.05% Triton X-100, and 1 mM EDTA. Dithionite was added to a final concentration of 5 mM to reduce the quinones.

RESULTS

Stimulated Emission Measurements. Figure 1A shows the decay of the 930-nm stimulated emission on the 20-ps

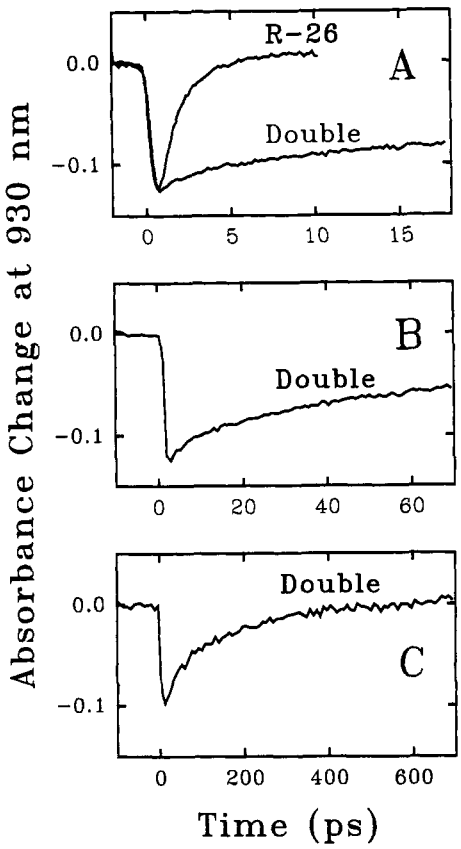

FIGURE 1: Decay of the stimulated emission at 930 nm and at a temperature of 20 K in quinone-reduced reaction centers isolated from *Rb. sphaeroides* strain R-26 and from the double hydrogen bond mutant [LH(L131)+LH(M160)]. Excitation was at 880 nm, and the relative polarization of the pulse and probe beams was the magic angle. Panel A shows a 20-ps absorption change time course for both R-26 and the double mutant. Panels B and C show 80- and 800-ps time courses, respectively, for the stimulated emission decay from the double mutant.

time scale from quinone-reduced reaction centers at 20 K. While the excited state from the R-26 reaction centers decays almost completely within 15 ps, only about 20% of the excited state from the double hydrogen bond mutant decays on that time scale. Panels B and C of Figure 1 show the decay of the stimulated emission in reaction centers from the double mutant on the 80- and 800-ps time scales, respectively. Many exponential decay terms with rate constants ranging from several picoseconds to hundreds of picoseconds would be required to accurately describe the decay of the stimulated emission in the double hydrogen bond mutant (see below for a description of decay times determined by exponential fitting).

Absorbance Spectra as a Function of Time. Figure 2 compares the absorption change spectra at several times for quinone-reduced reaction centers from R-26 and the double mutant. After the first 10 ps, there is very little change in the spectrum of R-26 reaction centers under these conditions (Figure 2A) as has been reported previously (Kirmaier & Holten, 1990; Vos et al., 1992). In contrast, spectral changes are observed even on the hundreds of picoseconds time scale in reaction centers from the double mutant, consistent with the kinetic traces in the stimulated emission region (Figure 1).

The spectral features observed in the 770–830-nm region both in the earliest time spectra and in the long-time spectra of Figure 2 also show interesting differences between R-26 and the double hydrogen bond mutant. The earliest time spectrum (at 400 fs; Figure 2A) in R-26 reaction centers shows

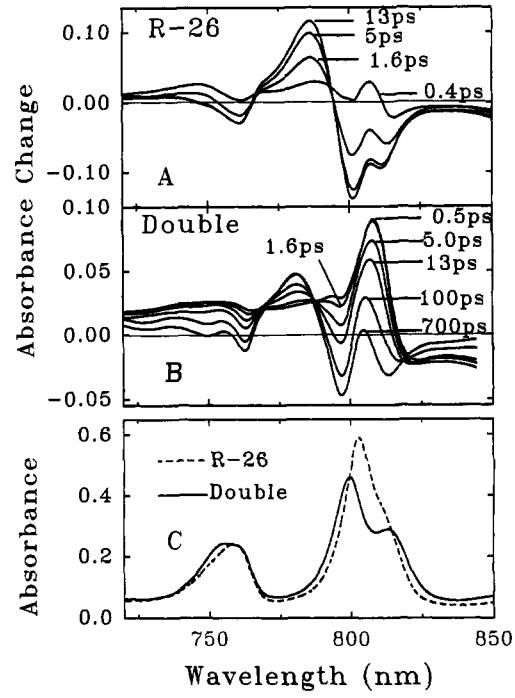

FIGURE 2: Time-resolved spectra of R-26 reaction centers (panel A) and reaction centers from the double hydrogen bond mutant (panel B). Excitation and polarization conditions were as in Figure 1. These spectra represent single time slices from a surface of absorption changes. For R-26 reaction centers, 100 spectra were taken at 0.15-ps intervals. For the double hydrogen bond mutant, 100 spectra were taken at 0.25-ps intervals, 100 spectra were taken at 0.8-ps intervals, and 100 spectra were taken at 8-ps intervals. Also shown are the ground-state absorption spectra of reaction centers from R-26 and the double hydrogen bond mutant taken at 20 K and normalized at 760 nm (panel C).

a very sharp but rather small absorbance increase near 810 nm. This has been interpreted as a change in the amount of intensity borrowing between P and the monomer bacteriochlorophylls upon P* formation (Nagarajan et al., 1993). A similar feature is seen in the earliest spectrum shown for the double hydrogen bond mutant (500 fs; Figure 2B), but it is several times larger and shifted slightly to lower energy. Following the above interpretation, this may indicate a larger intensity borrowing in the double mutant than in R-26. The longest time spectra are also quite different in the double hydrogen bond mutant and R-26. In R-26 reaction centers, one sees two poorly resolved absorption changes at roughly 803 and 813 nm (Figure 2A). These absorbance decreases have shifted farther apart in the double hydrogen bond mutant and are well resolved at 795 and 816 nm (Figure 2B). This is consistent with the additional resolution of transitions in this part of the ground-state low-temperature spectrum of the double hydrogen bond mutant (compare panels B and C of Figure 2).

The difference absorption spectra for both R-26 and the double hydrogen bond mutant always change in the same direction as a function of time. In addition, during the conversion of the excited singlet state present at early times to the charge-separated state present on long time scales, there are two isosbestic points (isosbestic, in this case, relative to the initial excited state) in the time-resolved spectra for both samples (at approximately 766 and 794 nm in R-26 reaction centers and at approximately 772 and 786 nm in the time-resolved spectra of the double hydrogen bond mutant; Figure 2A,B). These isosbestic points have previously been observed in R-26 reaction centers (Kirmaier & Holten, 1988). The presence of isosbestic points indicates that the system is starting

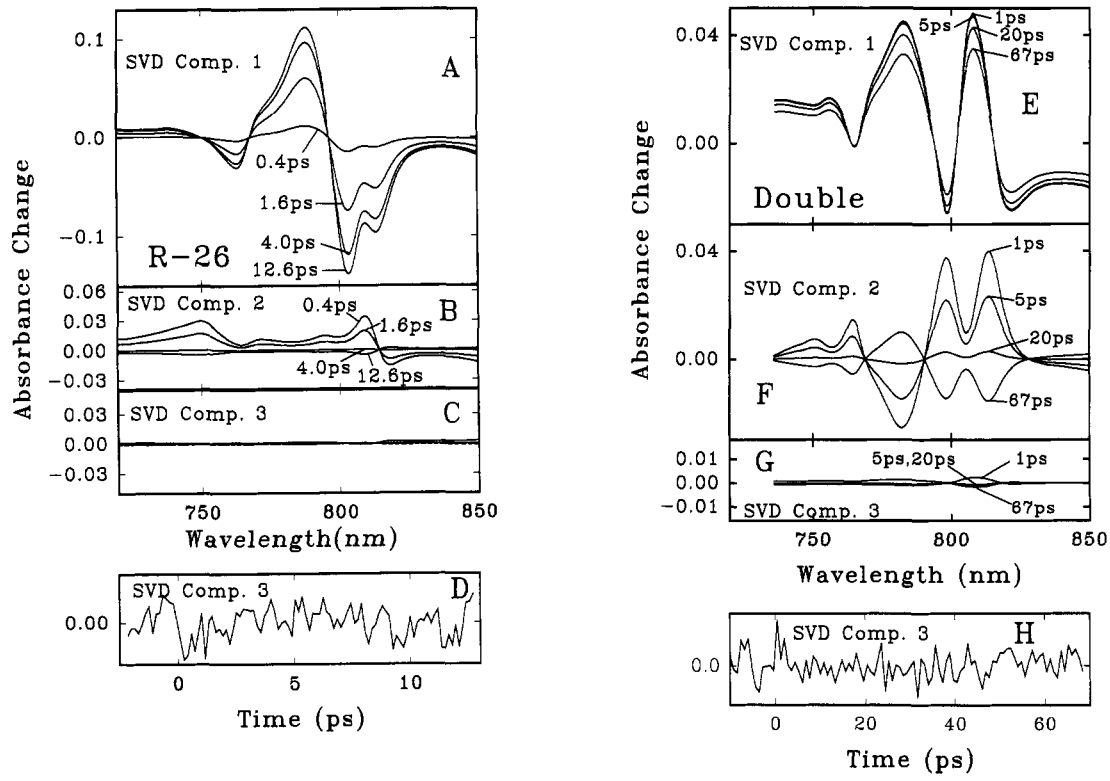

FIGURE 3: Singular value decomposition analysis of the time vs wavelength absorption change surface associated with electron transfer in R-26 (panels A–D) and double-mutant (panels E–H) reaction centers. The singular value decomposition was performed using the algorithms of Press et al. (1992). Panel A represents spectral slices through the portion of the time vs wavelength absorption change surface which is described by the matrix multiplication of the column vector representing the first spectral component of the singular value decomposition and the row vector representing the first temporal component weighted by the first diagonal element of the weighting matrix [see Press et al. (1992)]. Similarly, panels B and C are spectral slices through the surfaces defined by matrix multiplication of spectral and temporal vectors of the second (B) and third (C) components of the decomposition, respectively. It is important to note that the absorption change scale shown in these panels corresponds to the true absorption change associated with each singular value decomposition component. The sum of the surfaces represented by panels A, B, and C is exactly equal to the original time vs wavelength surface represented by the data in Figure 2A, minus a small contribution from the fourth and higher singular value decomposition components. Panel D is the orthonormal row vector associated with the third temporal singular value decomposition component. Panels E, F, G, and H correspond to panels A, B, C, and D, respectively, except that they represent the singular value decomposition results of the double mutant, [LH(L131)+LH(M160)].

in one state on the picosecond time scale and all subsequent spectra represent the progression toward a second state. This fact is particularly striking in the case of the double hydrogen bond mutant, where many different kinetic components are present on time scales from a few picoseconds to nearly a nanosecond, and yet the isosbestic points are maintained.

Spectral Component Analysis Using Singular Value Decomposition. The presence of isosbestic points alone is indicative of, but not quantitative evidence for, the existence of only two spectrally distinct states during the electron-transfer reaction. Isosbestic points in the difference spectra may not be maintained at early times during the excitation pulse or at long times due to ground-state recovery. In the double mutant, there appears to be a roughly 20% decrease in the absorbance change observed near 880 nm after 100 ps and a total decrease of about 30% in this bleaching after 700 ps. This may correspond to ground-state recovery on this time scale, though the measurements required to do a complete band-shape analysis have not been performed, and it is not clear what fraction of the absorption changes occurring on this time scale represent stimulated emission decay vs true ground-state recovery.

A quantitative method of determining the number of spectrally distinct components involved in the spectral evolution between the initial excited singlet state and the final charge-separated state is to analyze the absorbance change surface using singular value decomposition. This process describes a matrix (absorbance change values at various times and wavelengths in this case) in as few rows (spectral components) and columns (time courses) as possible and quantitates the contribution from each of the time/wavelength pairs of orthonormal vectors thus determined (Press et al., 1992). The results of such an analysis for R-26 reaction centers are shown in Figure 3A–D. Panels A, B, and C each show a particular spectral basis component weighted by its significance factor [the corresponding diagonal element of the **W** matrix in Press et al. (1992)] and by the value of the orthonormal temporal basis component at several different times. Another way of phrasing this is to say that, for each time/wavelength vector pair that resulted from the singular value decomposition, the portion of the original surface due solely to that pair was reconstructed, and Figure 3A–C shows spectral slices from those surfaces as a function of time. Figure 3D shows the orthonormal time vector for decomposition component 3. This component represents the time course of the third singular value decomposition spectral component. The vertical axis of this panel has the scale of the orthonormal basis set and cannot be compared directly to the scales in the upper panels. The time course of component 3 is primarily noise with a small feature near zero time that may represent a small effect of probe light wavelength dispersion on the analysis. It is important to emphasize that there is no *a priori* reason to assign the spectra in Figure 3A–C to any particular physically relevant state of the reaction center. These spectra are simply mathematically orthogonal basis components which, between them, describe the absorption change surface accurately. The

only physically meaningful information that comes directly from this analysis is the number of independent components which are required to describe the surface. As can be seen from Figure 3A–D, the absorption change surface for R-26 reaction centers is well described by only two spectrally distinct components. The size at any time of the third component compared to the other two is very small (the fourth and higher singular value decomposition components are all smaller than the third component), and it has a time course which is mostly random noise. Apparently, only the first two components represent nonrandom time-dependent spectral changes.

The singular value decomposition of the absorption change surface for the double mutant was also performed and is shown in Figure 3E–H. Again, there are primarily two linearly independent spectral components (Figure 3E,F), though in this case the third component (Figure 3G) appears more prominent than that observed for R-26 reaction centers. However, the time evolution of this minor third component is again essentially that of noise (Figure 3H). Thus, the spectrum of Figure 3G probably represents the noise spectrum of the transient absorption system. Notice that the overall absorption scale used to display the singular value decomposition spectral components (Figure 3E–G) for this mutant is 4-fold more sensitive than the scale used to display the R-26 spectral components of the decomposition. Therefore, it seems reasonable that the noise, which remains roughly constant in absolute magnitude, would appear larger in the decomposition analysis of the mutant. In fact, the absolute size of the third component in absorption change units is about the same between R-26 and the double mutant (Figure 3C,G). There may be a small contribution of this singular value decomposition component in the double mutant which is above the noise, but if so, it is only present during the first 2 or 3 ps of the time course (Figure 3H) and is only marginally statistically significant.

Exponential Decay Analysis. In order to assign physical meaning to component spectra such as those of Figure 3, one must analyze the absorption changes in terms of a physically meaningful basis set, in either the temporal or the spectral dimension. This is not accomplished by singular value decomposition alone. As a temporal basis set, exponential decays are normally employed. One possibility is to fit the temporal basis set from the singular value decomposition to a series of exponential decay terms and use the results of this to rotate the spectral basis set into a series of amplitude spectra which represent the spectral changes associated with each exponential decay term. Alternatively, one can directly analyze the entire surface by a global (multiwavelength) fit to a series of exponential components, directly obtaining the amplitude spectra from the fit. The latter approach was chosen for complete analysis because of its conceptual simplicity. Fitting of the singular value decomposition temporal components was also performed and gave very similar results.

Figure 4A shows the results of a multiwavelength analysis of R-26 reaction center transient absorption measurements taken at 20 K on the 15-ps time scale at 70 wavelengths between 720 and 850 nm (excitation at 880 nm). The absorption change surface was fit at all 70 wavelengths simultaneously to two exponential decay terms and a time-independent term:

$$\Delta A(\lambda,t) = \Delta a_1(\lambda)e^{-t/\tau_1} + \Delta a_2(\lambda)e^{-t/\tau_2} + \Delta a_3(\lambda) \quad (1)$$

where λ is the wavelength, t is the time, $\Delta A(\lambda,t)$ is the absorbance change surface, $\Delta a_i(\lambda)$ values are the wavelength-dependent preexponential amplitudes shown in Figure 3, and τ_i values are the lifetimes of the exponential decay components

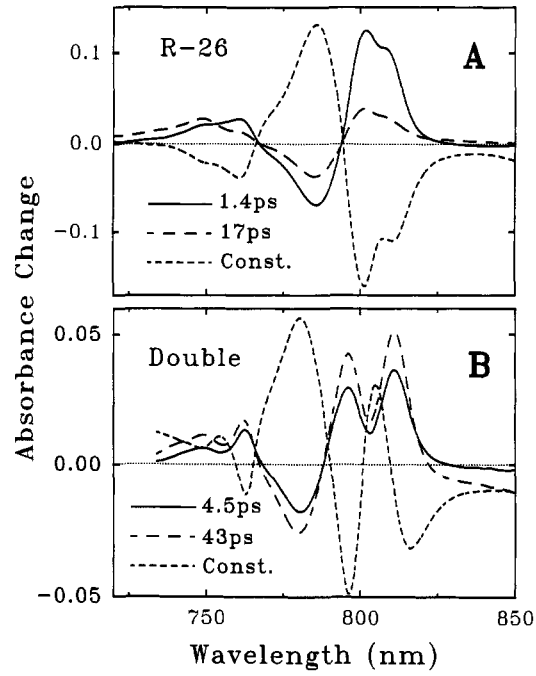

FIGURE 4: Preexponential amplitude spectra determined by fitting a time vs wavelength absorbance change surface to a sum of two exponential terms and a constant as described in the text. Seventy wavelengths were included in each fit over the wavelength region indicated. One hundred time points were collected at each wavelength. For R-26 reaction centers (panel A), the time points were spaced at 150 fs. For reaction centers from the double hydrogen bond mutant (panel B), the time points were separated by 800 fs. The times shown represent the decay times determined by the fit.

listed in Figure 3. Note that in this global analysis the τ_i values are wavelength-independent fitting parameters, while the $\Delta a_i(\lambda)$ values vary freely at each of the wavelengths in the analysis.

Using a single-exponential decay term to analyze the R-26 reaction center absorption change surface resulted in an inadequate fit with a χ^2 error that was 15% larger than that obtained with a two-exponential fit. Including a third exponential decay term in the fit over this time range did not significantly improve the χ^2. Over the time and wavelength ranges analyzed in the modeling presented below, the fitting curves remained within the range of the noise (about ±0.003 absorbance units). The two decay times, τ_1 and τ_2, identified by the fit for R-26 reaction centers were 1.4 ± 0.2 and 17 ± 4 ps. The errors shown for the time constants are estimated from analyzing the individual runs, which were averaged for the fit shown in Figure 4A.

Figure 4B shows the amplitude spectra, $\Delta a_i(\lambda)$, resulting from an analysis of the double hydrogen bond mutant by fitting the time vs wavelength absorption change surface with two exponential decay terms and a constant, just as was done for R-26 reaction centers. In this case, data were analyzed on an 80-ps time scale. The fitting parameters derived from fits of the double hydrogen bond mutant data depend on the time scale over which the fit is performed, the number of exponentials included in the fit, and the region of the decay included in the fit. Thus, it is not accurate to assign each decay term to a distinct spectral intermediate. Instead, each amplitude spectrum in Figure 4B represents a distribution of amplitude spectra associated with a distribution of time constants. On the 80-ps time scale, two decay times of 4.5 ± 0.5 and 43 ± 5 ps resulted from the fit. As with the R-26 data, this was an adequate description of the decay to within the noise of the measurement (±0.001 optical density units).

The two resolved absorption changes centered at approximately 797 and 816 nm in the double hydrogen bond mutant are kinetically indistinguishable on the time scales measured. Fits were also performed on data taken over 20 or 800 ps (data not shown). In the case of a 20-ps time scale, the decay fit well to a 7.8-ps exponential decay term and a constant, and on the 800-ps time scale the decay rates that resulted were 38 and 200 ps in addition to a constant term. As has been described for the fluorescence decay kinetics from this mutant (Peloquin et al., 1994), one would expect the time constants resulting from exponential fits to depend on the data collection time scale if there were more kinetic components in the charge-separation process than could be resolved given the signal-to-noise in the data. The preexponential amplitude spectra of all of these decay components, except for the 200-ps component, are similar in shape, though the magnitude changes. The 200-ps component has a somewhat different amplitude spectrum, since on this time scale there occurs not only charge separation but apparently some ground-state recovery as well.

DISCUSSION

The central results of this study are that the decay of P* in the double mutant is visible by transient absorption techniques for hundreds of picoseconds and has a complex, multiexponential kinetic profile throughout this time period. However, in contrast to the complexity of the kinetics, the spectral description of the absorbance changes is simple; only two spectrally distinct states have been identified by singular value decomposition analysis (Figure 3). Both this study and the work by others cited above indicate that a similar situation also exists in R-26 reaction centers, as well as at physiological temperatures, though the spectral characteristics of the P*/$P^+H_A^-$ mixture cannot be as accurately assessed on time scales longer than 10 ps as they can in the double mutant.

Models Involving Intermediate Excited or Charge-Separated States. One of the proposals to account for the multiexponential kinetics of absorption and emission measurements both during the first few picoseconds (Holzapfel et al., 1989) and on the 10-ps time scale [Hamm et al., 1993; also discussed by Muller et al. (1992) and Du et al. (1992)] is the involvement of additional excited or charge-separated states in the reaction. One can see from the singular value decomposition analysis of Figure 3 that the kinetic complexity in the absorption changes in R-26 reaction centers does not involve a substantial contribution from more than two spectrally distinct states at 20 K. There is a small contribution from the third component of the singular value decomposition analysis (Figure 3C). However, its magnitude is only about 2% of the large absorption changes associated with the first singular value decomposition component (Figure 3A), and it has a time course which indicates that it is primarily due to random noise.

The double-mutant reaction centers also show only two spectrally distinct components that appear to be involved in the electron-transfer reaction at 20 K. The size and spectrum of the third spectral component of the singular value decomposition are those of the inherent kinetic noise in the transient absorption apparatus (Figure 3G), a conclusion which is supported by the nearly random time course of this component (Figure 3H). These observations argue strongly against the suggestion of Hamm et al. (1993) that population of the state $P^+B_B^-$ causes the multiexponential decay of P*, at least at low temperature.

Given the reaction center structure, it is natural to suppose that the electron resides on B_A during transfer from P* to $P^+H_A^-$. However, from various spectroscopic studies of electron transfer, it is clear that if the state $P^+B_A^-$ is populated at all, the fraction of the population in this state is never more than about 15% at room temperature [reviewed by Kirmaier and Holten (1993)], and considerably smaller at low temperature as indicated by the singular value decomposition analysis of Figure 3 and previous studies (Kirmaier & Holten, 1993). In fact, the magnitude of the absorption changes represented by the third and higher singular value decomposition components in R-26 reaction centers never total more than a few percent of the size of the long-lived absorption changes associated with $P^+H_A^-$. If one assumes that $P^+B_A^-$ involves absorption changes which are similar in magnitude to those of $P^+H_A^-$, then one would have to conclude that only a few percent of this state is present at any time at low temperature. Those investigators who have considered the possibility that $P^+B_A^-$ is a populated reaction intermediate between P* and $P^+H_A^-$ have usually interpreted this in terms of a kinetic model in which $P^+B_A^-$ decays faster than it is formed (Holzapfel et al., 1989). However, in this model, the population of $P^+B_A^-$ relative to other states in the system is determined by the ratio of the first and second electron-transfer reactions in the following scheme:

Scheme 1

$$P^* \xrightarrow{k_1} P^+B_A^- \xrightarrow{k_2} P^+H_A^-$$

where $k_2 > k_1$ and the relative steady-state concentration of $P^+B_A^-$ is approximately $(k_1/k_2)[P^*]_0$ at early times, where $[P^*]_0$ is the initial population of the excited singlet state. Since in R-26 reaction centers most of the charge separation occurs with a time constant of about 1.4 ps, k_1 must be at least that fast. Given that $P^+B_A^-$ has a relative steady-state concentration of only a few percent, k_2 in this model would have to be on the order of tens of femtoseconds, much faster than any known electron-transfer reaction over a similar distance. This makes Scheme 1 an unlikely description of the electron-transfer events at low temperature, in agreement with previous conclusions [reviewed by Kirmaier and Holten (1993)].

Dynamic Solvation Model. If the complex kinetic decay of P* is not due to the involvement of multiple excited or charge-separated states, then it probably arises from the involvement of multiple nuclear configurations of the system. Static heterogeneity of the reaction center nuclear configuration has been considered by others as a possible explanation for the complex absorption change kinetics both on very early time scales (the first few picoseconds; Kirmaier & Holten, 1990; Muller et al., 1992; Du et al., 1992) and on the time scale of the second electron-transfer reaction (hundreds of picoseconds; Kirmaier & Holten, 1990; Kirmaier et al., 1985). As will be described below, it is possible that some of the early time kinetic complexity could be explained in this way. However, the P* decay on the 100-ps and longer time scale appears to be due to thermal repopulation of the excited state from the charge-separated state and is best described as a dynamic progression of reaction center conformations (Peloquin et al., 1994; Woodbury & Parson, 1984). Thus, the results reported here are first analyzed as a straightforward extension of the dynamic solvation model, followed by a consideration of the effects of energy or rate distributions in the reaction center population.

Suppose that P* is formed initially by light absorption and approaches thermodynamic equilibrium with the charge-separated state $P^+H_A^-$ within a few picoseconds. Initially, in this model, P* and $P^+H_A^-$ are nearly degenerate in energy,

and thus, there is a substantial equilibrium population of P* on the time scale of the microscopic rate constants for electron transfer. The rate-limiting step in the complete transfer of the electron from P to H_A is the reorganization of the nuclear configuration of the system (presumably the protein). These conformational changes stabilize the charge-separated state, and as time passes a larger and larger fraction of the reaction centers are in the state $P^+H_A^-$. The nuclear reorganization involves many different conformational changes which occur on time scales from picoseconds to nanoseconds.

This model provides a possible explanation for the complex kinetic behavior of the state P*. The fact that the decay of P* is multiexponential is explained by a decrease in the equilibrium population of the excited state upon each conformational change favoring the charge-separated state. The fact that the amplitudes of the long-lived decay components of P* are increased in a mutant that increases the oxidation potential of P is due to the fact that the free energy gap between each of the conformational intermediates and P* is smaller in the high-potential mutant, giving rise to more thermal repopulation of P*.

Calculation of Intermediate Spectra Using Kinetic Models. A kinetic analysis based on the dynamic solvation model can be used to determine the spectral characteristics of the reaction center conformational states involved in the model. In this analysis, the time course is described in terms of a series of first-order chemical reactions (Scheme 2), and it is possible to determine the spectrum of each state involved in the reaction by analyzing the time vs wavelength surface.

Scheme 2

$$A \underset{k_{21}}{\overset{k_{12}}{\rightleftharpoons}} B \underset{k_{32}}{\overset{k_{23}}{\rightleftharpoons}} C$$

In Scheme 2, A is the initial state of the system after light absorption (P* in the dynamic heterogeneity model), B is a kinetic intermediate (an initial form of $P^+H_A^-$ in the model), and C is the final state (a relaxed form of $P^+H_A^-$ in the model). Note that this simple scheme assumes nothing about the spectral nature of A, B, and C, nor does it assume anything about the time scale upon which equilibrium is achieved between these states. It does assume that the reaction starts entirely in A and that only three states are involved. Restricting the number of total states to three is probably an oversimplification of the dynamic heterogeneity model. Each of the amplitude spectra in Figure 4 may well represent the average spectral change for several unresolved steps in the transition between the excited state and the final charge-separated state. However, this approximation should not greatly affect the overall conclusions drawn from the kinetic analysis, since the question being asked is, are the spectral characteristics of the intermediate states consistent with a transition from P* to $P^+H_A^-$ and subsequent relaxation of the charge-separated state? As long as only two spectrally distinct states are involved (the excited state and the charge-separated state, as is implied by Figure 3), the spectra associated with each of the kinetic intermediates after charge separation should be roughly the same, independent of the time scale of the measurement, the number or precise value of the exponential decay times determined from the fits, or the number of intermediates used in the model. The only parameters which are free in this calculation are the relative free energies of the three states.

In the case of the double mutant, there is some question about which time scale to perform the analysis on, since the decay occurs on time scales from picoseconds to hundreds of picoseconds (Figure 1). The 80-ps time scale was chosen since this time scale was fast enough to resolve the evolution of the absorbance changes on the few picoseconds time scale, but long enough to include most of the charge-separated state formation. Inclusion of longer times would have required the consideration of ground-state recovery in the model, introducing a third spectrally distinct state into the analysis.

The calculation of the difference extinction coefficient spectra for each state is performed as follows. The absorbance change dependence on the wavelength and time, $\Delta A(\lambda,t)$, is given by

$$\Delta A(\lambda,t) = C_A(t)\Delta\epsilon_A(\lambda) + C_B(t)\Delta\epsilon_B(\lambda) + C_C(t)\Delta\epsilon_C(\lambda) \quad (2)$$

where the $C_i(t)$ values are the concentrations of the three states as a function of time and the $\Delta\epsilon_i(\lambda)$ values are the difference extinction coefficients for each state. One can then solve the differential equations describing the chemical reactions of Scheme 2 and determine the $C_i(t)$ values in terms of the microscopic rate constants, k_{ij}, and the initial concentrations of the three states. By equating eqs 1 and 2, the microscopic rate constants can be related to the observed decay times, τ_i, and the difference extinction coefficients can be expressed in terms of the preexponential amplitude spectra of Figure 4, $a_i(\lambda)$, and the microscopic rate constants of Scheme 2. The solution, however, is underdetermined, and in order to obtain spectra for each of the states in Scheme 2, the relative free energies of the three states must be specified.

Since the relative free energies of the states in Scheme 2 are free parameters, the simplest assumption to make would be that the free energy gaps between the states are large relative to k_BT (the thermal energy of the system). This is often a good assumption at 20 K, since even very small enthalpy gaps on the order of 100 cm^{-1} are enough to make reactions nearly irreversible. In the irreversible case ($k_{12} \gg k_{21}$, $k_{23} \gg k_{32}$), the solutions to the kinetic equations governing the time dependence of the concentrations of the three states in Scheme 2 are simple. If one assumes that the initial concentration of state A (presumably P*) is 1.0,

$$C_A(t) = e^{-k_{12}t} \quad (3a)$$

$$C_B(t) = \frac{k_{12}}{k_{23} - k_{12}}(e^{-k_{12}t} - e^{-k_{23}t}) \quad (3b)$$

$$C_C(t) = -\frac{k_{23}}{k_{23} - k_{12}}e^{-k_{12}t} + \frac{k_{12}}{k_{23} - k_{12}}e^{-k_{23}t} + 1.0 \quad (3c)$$

By substituting these expressions into eq 2 and equating each to eq 1, one can see that

$$a_1(\lambda) = \Delta\epsilon_A(\lambda) + \frac{k_{12}}{k_{23} - k_{12}}\Delta\epsilon_B(\lambda) - \frac{k_{23}}{k_{23} - k_{12}}\Delta\epsilon_C(\lambda) \quad (4a)$$

$$a_2(\lambda) = -\frac{k_{12}}{k_{23} - k_{12}}\Delta\epsilon_B(\lambda) + \frac{k_{12}}{k_{23} - k_{12}}\Delta\epsilon_C(\lambda) \quad (4b)$$

$$a_3(\lambda) = \Delta\epsilon_C(\lambda) \quad (4c)$$

Solving for the difference extinction coefficients,

$$\Delta\epsilon_A = a_1(\lambda) + a_2(\lambda) + a_3(\lambda) \quad (5a)$$

$$\Delta\epsilon_B = -\frac{k_{23} - k_{12}}{k_{12}} a_2(\lambda) + a_3(\lambda) \quad (5b)$$

$$\Delta\epsilon_C = a_3(\lambda) \quad (5c)$$

Note that by making the assumption that the initial concentration of the excited singlet state, $C_A(0)$, is 1, the $\Delta\epsilon_i$ values determined from eqs 5a–c are relative difference extinction coefficients and have arbitrary units. The $\Delta\epsilon_i$ values obtained from these calculations are shown in Figure 5.

For R-26 reaction centers with irreversible kinetics (Figure 5A), the B and C states have very similar spectral features, as would be expected if they represented nearly identical charge-separated states with different nuclear free energies. Given that these are relative extinction coefficient spectra, one would expect that not only the shapes but the magnitudes of the spectra of the different forms of the charge-separated state would match. The magnitudes of the B and C spectra are similar, but they clearly differ by more than the error in the measurement. Looking at the $\Delta\epsilon$ spectra for the double mutant in Figure 5B, the state B and state C spectra have some similar features, but they are not nearly as similar in shape as the corresponding spectra for R-26. There are clearly shifts in the spectral peaks between the two states, and the relative sizes of, for example, the absorbance increases near 780 and 810 nm are different in the B and C spectra of the double mutant. Given the presence of the common crossing points at approximately 770 and 788 nm in the $\Delta\epsilon$ spectra for the double mutant, it is unlikely that the A, B, and C spectra shown are linearly independent (i.e., this implies that one of these states is actually a linear combination of the other two). In fact the spectrum for state B in this figure is approximately what would be obtained by averaging the other two spectra.

The dynamic heterogeneity model described above requires that states B and C, which are different nuclear configurations of the same charge-separated state, have very similar $\Delta\epsilon$ spectra, in both form and magnitude. In principle, if the spectra shown in each panel of Figure 5 all arise from linear combinations of only two independent spectra, it should be possible to pick values for the standard free energy differences between the three states such that the B and C states have identical spectra. This is because introducing back reactions in the differential equations that govern Scheme 2 results in A, B, and C spectra which are linear combinations of the spectra obtained if irreversible reactions are assumed. The procedure for solving the case including back reactions and deriving the relative extinction coefficient spectra is similar to that described for the irreversible case, though algebraically more complex. The relative free energies between the states were selected by varying them as free parameters and attempting to match both the shape and the magnitude of the spectra for the B and C states, thus resulting in only two spectrally distinct states in the system as demonstrated by the singular value decomposition analysis of Figure 3. The results of these calculations are shown in Figure 6. For reaction centers from both R-26 and the double mutant it was possible to select relative free energies which resulted in only two spectrally distinct states. Note that, in order to generate nearly identical B and C spectra, the standard free energy differences between the three states in both R-26 and the double mutant must be very small (less than 25 cm^{-1}; Figure 6) relative to values reported at higher temperatures and at longer times (Woodbury & Parson, 1984; Goldstein et al., 1988; Ogrodnik et al., 1988; Muller et al., 1992; Williams et al., 1992a). This is consistent with a concept inherent in the dynamic solvation

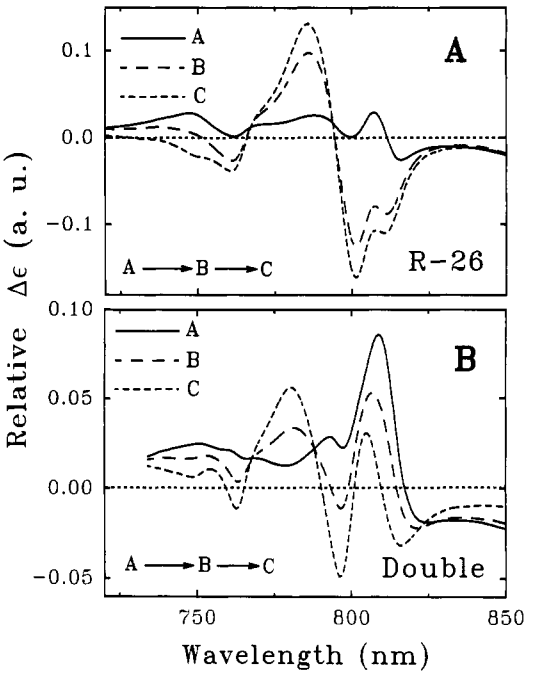

FIGURE 5: Wavelength dependence of the relative difference extinction coefficients ($\Delta\epsilon$) calculated for the states in Scheme 2. Panel A shows the results for R-26 reaction centers; panel B shows the results for reaction centers from the double mutant. The spectra shown represent the calculated $\Delta\epsilon$ spectra of the indicated states using a model involving irreversible reactions between A, B, and C in Scheme 2 (P^*, $P^+H_A^-$, and a relaxed form of $P^+H_A^-$, respectively, in the dynamic heterogeneity model).

model; the free energy gaps between these states must be on the order of k_BT or smaller for repopulation of P* to occur and result in the complex kinetic decay of the system.

The values of the free energy gaps used in Figure 6 to cause the B and C spectra to overlap are not unique for reaction centers from either R-26 or the double mutant. In both cases, the value of the standard free energy gap for the first reaction can be varied by roughly 10 cm^{-1} in either direction as long as the value for the second reaction is changed in a compensatory manner.

Calculation of Kinetic Decays Using a Spectral Model. The kinetic scheme used above to calculate the spectra of intermediate states assumes that one can identify a kinetic basis set, exponential decay terms in this case, and describe the observed data in terms of that basis set. The basis set is then analyzed in terms of a kinetic model which assumes a small number of exponential first-order decay constants.

Given the detailed time vs wavelength absorption change surface measured as part of this work, one could also describe the data in terms of a spectral basis set. The singular value decomposition analysis of Figure 3 indicates that there are only two spectrally distinct states involved in the electron-transfer reaction. It would therefore be reasonable to pick two spectra representing the initial and final states and to fit the rest of the spectra at intermediate times to a linear combination of those two spectra. From these fits one could obtain the relative concentrations of the initial state (P^*) and the final state ($P^+H_A^-$) as a function of time. The fit relates $A(\lambda,t)$ to the relative difference extinction coefficient spectra of the excited singlet state and the final charge-separated state on the time scale of the measurement:

$$A(\lambda,t) = C_I(t)\Delta\epsilon_I(\lambda) + C_F(t)\Delta\epsilon_F(\lambda) \quad (6)$$

where $C_I(t)$ and $C_F(t)$ are the concentrations of the initial and

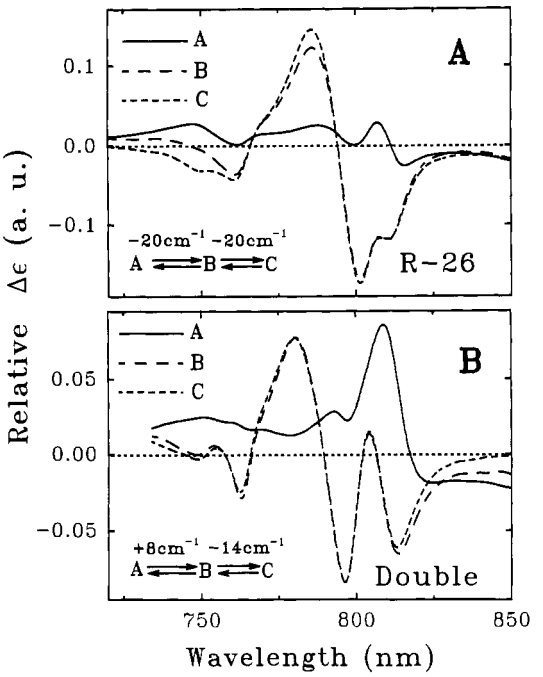

FIGURE 6: Relative difference extinction coefficient ($\Delta\epsilon$) spectra calculated by assuming reversible reactions between states A, B, and C in Scheme 2. For R-26 reaction centers (panel A), the driving force for each reaction was set to -20 cm^{-1}. The microscopic time constants obtained from the model were 1.9 ps for the forward time constant of the first reaction, 6.1 ps for the backward time constant of the same reaction, 18 ps for the forward time constant of the second reaction, and 57 ps for the backward time constant of this reaction. For reaction centers from the double mutant (panel B), an 8 cm^{-1} standard free energy gap was used for the first step and a -14 cm^{-1} gap was used for the second step. The microscopic time constants calculated for the reversible reactions were 14 and 8 ps for the forward and backward time constants of the first step, respectively, and 28 and 74 ps, respectively, for the forward and backward time constants of the second step.

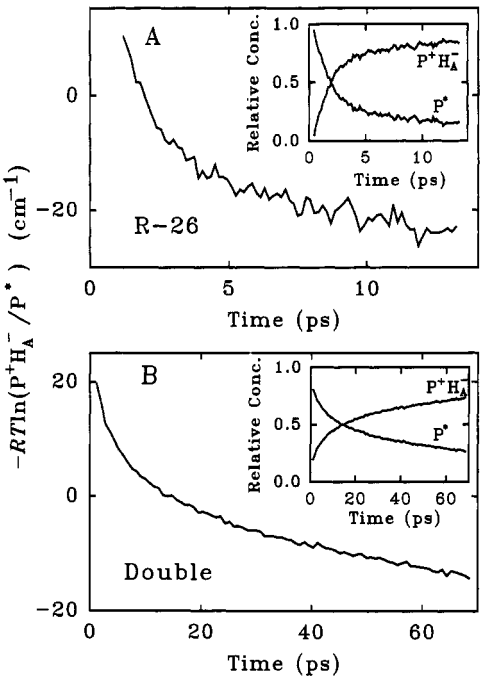

FIGURE 7: Results of fitting the absorption change surface for (A) R-26 reaction centers and (B) double hydrogen bond mutant reaction centers with a linear combination of spectra representing the initial and final states. The fit was constrained to a single parameter by assuming that the total concentration of the two species did not change with time. For R-26 reaction centers (panel A), the 0.4-ps spectrum shown in Figure 2 was used as the initial state (presumably P*). The amplitude spectrum of the constant term in Figure 3A was used as a representation of the spectrum of the final state (presumably $P^+H_A^-$). For the double hydrogen bond mutant (panel B), the 0.5-ps spectrum of Figure 2 was used for the initial state (P*) and the 700-ps spectrum was used for the final state ($P^+H_A^-$). The largest fitting errors (in terms of the calculated curve minus the observed spectrum) were no more than 5% of the total signal. Each time point represents an independent fit of a time-resolved spectrum. The figure insets show the relative concentrations of P* and $P^+H_A^-$ as a function of time calculated from the fit. The main panels show the standard free energy gaps between the initial and final states calculated as $-RT\ \ln([P^+H_A^-]/[P^*])$.

final spectrally distinct states as a function of time and $\Delta\epsilon_I(\lambda)$ and $\Delta\epsilon_F(\lambda)$ are the relative difference extinction coefficient spectra of the two spectrally distinct states. If one had infinite time resolution and could take spectra for an arbitrarily long time after the excitation, one would define

$$\Delta\epsilon_I(\lambda) = \Delta A(\lambda,0) \tag{5d}$$

and

$$\Delta\epsilon_F(\lambda) = \Delta A(\lambda,\infty) \tag{5e}$$

In the fit performed here, the basis spectra were taken from the early and long time absorption change spectra as defined in the caption to Figure 7. The absorbance change spectra at each time were then fit independently, allowing the coefficients $C_I(t)$ and $C_F(t)$ to vary as fitting parameters and holding the spectral shapes of $\Delta\epsilon_I(\lambda)$ and $\Delta\epsilon_F(\lambda)$ constant for all t. $C_I(t)$ and $C_F(t)$ were not independent fitting parameters since at all times the sum of the two concentrations was held constant. This final constraint assumes no yield loss (ground-state recovery) on the time scale of the measurement. This is a very good approximation for R-26 reaction centers. For the double mutant there is probably a yield loss of roughly 20% on the 80-ps time scale, though a complete yield analysis has not been done. In any case, fitting the data from this mutant on the 80-ps time scale while either holding or not holding the sum of the concentrations of the initial and final states constant made little difference in the qualitative features of the concentration time courses determined.

The results of such a set of fits for both R-26 and the double hydrogen bond mutant are shown in the insets to Figure 7. The predicted time courses of P* decay for the two samples are consistent with the decays of the stimulated emission shown in Figure 1, and like the stimulated emission decays, the time course determined for P* in each of the reaction centers cannot be described by a single-exponential decay term. Note that the stimulated emission region of the spectrum was not included in these spectral fits, only the 700–850-nm region, so the correspondence of the calculated P* time courses and the stimulated emission decays is not forced. This method of analysis presupposes knowledge of the spectra of the initial and final states; however, it has the advantage that it assumes nothing about the kinetics of the time courses of the two states involved.

If one assumes that dynamic solvation is the source of the complex kinetic decay of P*, the spectral analysis described above can be taken one step further by assuming that after a few picoseconds the two states, P* and $P^+H_A^-$, are in thermodynamic equilibrium. Note that this is *not* assumed in the calculations of free energy changes in the kinetic analysis of the solvation model described above. This assumption is, however, inherent in the dynamic solvation model. After all, if electron transfer *per se* was the rate-limiting step involved on the time scales under investigation, then the decay of P* would not be multiexponential. The complexity of the kinetics

in this model depends on the nuclear conformational relaxations being rate limiting. As long as electron transfer is fast compared to the conformational relaxations, the relative populations of P* and the charge-separated state should achieve near-equilibrium levels rapidly. Thus, the dynamic solvation model predicts that one should be able to calculate the standard free energy change between P* and $P^+H_A^-$ as a function of time from the concentrations of P* and $P^+H_A^-$ given in the insets to Figure 7. The time dependence of the standard free energy gap calculated as $-RT \ln([P^+H_A^-]/[P^*])$ is shown in the main panels of Figure 7 for R-26 (panel A) and the double hydrogen bond mutant (panel B).

Exactly when one chooses to equate the expression $-RT \ln([P^+H_A^-]/[P^*])$ in Figure 7 to the free energy difference between P* and $P^+H_A^-$ depends on how fast one believes the charge separation occurs and thermodynamic equilibrium between the states is achieved. If the assumption is made that equilibration has been achieved within a few picoseconds, one finds good agreement between the kinetic analysis of Figure 6 and the spectral analysis of Figure 7. In R-26 reaction centers, the spectral analysis of Figure 7A indicates that after 4 or 5 ps a standard free energy gap of about -15 cm^{-1} has developed. This is in agreement with the driving force calculated for the first kinetic step in Figure 6A of -20 cm^{-1}. For the double hydrogen bond mutant, the kinetic analysis of Figure 6B predicts a standard free energy gap that is initially slightly positive at times earlier than about 15 ps and then becomes slightly negative on the tens of picoseconds time scale. This is essentially what is predicted by the spectral analysis of Figure 7B. If one continues the spectral analysis out to several hundred picoseconds, the free energy gap between P* and $P^+H_A^-$ continues to become more negative until after about 300 ps it is roughly -40 cm^{-1} for the double hydrogen bond mutant (data not shown).

Though the studies in this report were performed at low temperature, and though the most extreme example of the complex kinetic decay of P* presented utilized a mutant, multiexponential behavior of the excited-state decay has been observed at room temperature in R-26 reaction centers as well. This is true on the 10-ps time scale (Du et al., 1992; Muller et al., 1992; Hamm et al., 1993) as well as on longer time scales (Schenck et al., 1982; Woodbury & Parson; 1984; Williams et al., 1992a; Muller et al., 1992; Peloquin et al., 1994). If this complex kinetic behavior is interpreted as dynamic solvation, one finds that on the few-picoseconds time scale the driving force for electron transfer at room temperature is on the order of 300 cm^{-1}. This number was calculated from the ratio of the amplitudes of the 2- and 10-ps decay components reported by Du et al. (1992). Thus, at physiological temperatures in wild-type reaction centers, application of the dynamic solvation model results in very low driving forces for electron transfer, compared to measurements performed on longer time scales (Schenck et al., 1982; Woodbury & Parson, 1984; Williams et al., 1992a; Ogrodnik et al., 1988; Goldstein et al., 1988) or compared to electron-transfer reactions studied in solution (Closs & Miller, 1988).

Static Heterogeneity in the Free Energy of P and $P^+H_A^-$.* The standard free energy calculated between P* and $P^+H_A^-$ using the dynamic solvation model is surprisingly small even on the nanosecond time scale (Peloquin et al., 1994), and it is nearly zero on the picosecond time scale. This is difficult to reconcile with the traditional nonadiabatic electron-transfer concepts normally used to describe the early reactions of bacterial photosynthesis (see below). While there is good evidence that the fluorescence detected on the nanosecond time scale is due to thermal repopulation of the excited singlet state (Peloquin et al., 1994), it is quite possible that some of the complexity of the decay kinetics observed on the picosecond time scale is due to static heterogeneity in the reaction center population, resulting in a distribution of initial electron-transfer rates. If this is true, then the kinetic complexity of the P* decay at 20 K would not be the result of a $P^*/P^+H_A^-$ standard free energy gap which is tens of wavenumbers on the picosecond time scale, but rather simply the sum of many distinct reaction centers in the population undergoing electron transfer at different rates. This idea has been developed extensively in the past to describe both the multiexponential behavior of the fluorescence decay and the kinetic complexity of the transient absorption changes associated with the $P^* \rightarrow P^+H_A^-$ reaction (Kirmaier & Holten, 1990; Du et al., 1992; Muller et al., 1992). In fact, one would expect that the dynamic conformational heterogeneity that results in a time-dependent solvation of the charge-separated state on longer time scales would also give rise to a static distribution of $P^+H_A^-$ free energies on time scales that are shorter than the rate of the conformational changes.

A kinetic model based on static heterogeneity can be applied to the amplitude spectra of Figure 4, and the spectra and populations of the states involved can be calculated. In this model there are two or more kinetically distinguishable types of reaction centers as depicted in Scheme 3.

Scheme 3

$$A_1 \xrightarrow{k_1} B_1$$

$$A_2 \xrightarrow{k_2} B_2$$

Here A_1 and A_2 are two conformational forms of the initial excited singlet state and B_1 and B_2 are two conformational forms of the charge-separated state. Since only two spectrally distinct states were found to be present during the reaction (Figure 3), one must conclude that the different conformations of reaction centers are not spectrally distinct in either the initial or charge-separated states. This makes the determination of the spectra of each species trivial. The spectrum observed at early time is the spectrum of both A_1 and A_2 (see the early time spectra of Figure 2), and the spectrum at long time is the spectrum of both B_1 and B_2 (see the long time spectra of Figure 2). One can also determine the relative amounts of the two reaction center conformers from the kinetics. The relative amounts of the two conformational forms of the reaction center shown in Scheme 3 (a three-exponential decay requires two reaction center conformations in this model) are given by the ratio of the amplitudes of the two exponential decay components observed. In R-26 the two forms are present in a ratio of roughly 4:1; in the double mutant the ratio of the two forms is nearly 1:1.

It is important to realize that, while the static heterogeneity model could play a role in the complex kinetics on the picosecond time scale, it cannot be used to explain the longer-lived (100 picosecond to nanosecond) components of the P* decay which have been observed (Peloquin et al., 1994). This means that whether or not there is static heterogeneity in the reaction center population, one must still conclude that the magnitude of the standard free energy gap between P* and $P^+H_A^-$ is 200 cm^{-1} or less at 20 K, particularly in the high-potential mutants. Thus, though there is no way to argue against static heterogeneity in the reaction center at early times, there is no compelling reason to include it in the present

model either. The real question is, how can electron transfer occur at all with such small driving forces?

Adiabatic Electron Transfer in the Bacterial Reaction Center. Studies of electron transfer in small organic molecules typically yield estimates of internal reorganization energies associated with charge separation on the order of a few thousand wavenumbers [e.g., Closs and Miller (1988)]. In large conjugated π systems such as bacteriochlorophyll and bacteriopheophytin, one would expect somewhat smaller internal reorganization energies since the addition or removal of an electron would not represent as large a perturbation as it would in a smaller molecule. Dominant mode frequencies and coupling constants have been calculated for the special pair from structural models (Warshel, 1980), and one can use these to estimate an internal reorganization energy, $\lambda_v = \sum_i S_i\omega_i$, where the ω_i values are the frequencies of the modes involved and the S_i values are the coupling constants (Huang-Rhys factors) as described in Alden et al. (1992). For the P* to $P^+H_A^-$ reaction, an estimate of approximately 700 cm^{-1} can be obtained by combining vibrational reorganization energies for the P to P*, P to P^+, and H_A to H_A^- reactions. This estimate is considerably larger than the driving force for electron transfer obtained above on the picosecond time scale. Traditional nonadiabatic electron-transfer theory suggests that if the reorganization energy is large compared to the driving force for the reaction, a substantial activation energy for the reaction should result [e.g., Closs and Miller (1988)]. Given the fast rate of electron transfer at low temperature in R-26 reaction centers, and even in the high-potential mutants, it is clear that no significant activation barrier exists. (As shown in Figure 4, about half of the P* decay in the double mutant occurs with a 4-ps time constant, and in another high-potential mutant, LH(L131), which was described in the accompanying paper (Peloquin et al., 1994), the majority of the P* decay at low temperature has a time constant of about 4 ps.)

The dynamic solvation model suggests that the relative populations of P* and $P^+H_A^-$ are controlled, at least on some time scales, not by the microscopic rate of electron transfer but instead by the rate at which the nuclear configuration of the system can change toward a conformation which is more favorable for the charge-separated state. One could take this concept to the extreme and apply it during the first few picoseconds when most of the charge separation occurs in wild-type reaction centers. If the rate of electron transfer is controlled by the rate of nuclear movements in the system, then the reaction is effectively adiabatic. In fact, many of the results and calculations presented in this work and in the accompanying paper are more consistent with adiabatic electron transfer near the strong coupling limit than they are with traditional nonadiabatic electron transfer between states which come to rapid thermal equilibrium with the bath (strong coupling refers to conformations near the crossing point between the zero-order potential surfaces of the reactant and product states). In this view, the potential along the reaction coordinate connecting P* and $P^+H_A^-$ can be described by a single, continuous surface. This allows for a relatively large time-dependent displacement (reorganization) with a small overall decrease in free energy and very little activation energy.

The small activation energy implies that the overall potential surface described by interaction between the zero-order potential surfaces of P* and the charge-separated states never has a significantly positive slope in the direction from P* to $P^+H_A^-$. This can be accomplished in several possible ways. One could suppose that the zero-order potential surfaces of the reactant and product states cross near the minimum of the unperturbed reactant potential surface. However, given the relatively small effect of increasing the P/P^+ potential on the temperature dependence of the electron-transfer rate (at least half of the P* decay in the double mutant still takes place on the few-picoseconds time scale at 20 K), it seems unlikely that the exact position that the zero-order surfaces cross is critical. It is also possible that the reactant zero-order potential surface is very shallow relative to the product surface, allowing large changes in the relative free energy of the charge-separated state with little change in the energy of the crossing point between the zero-order potential surfaces. Another way of generating a smooth surface between P* and $P^+H_A^-$ is to assume that the coupling between P*, $P^+B_A^-$, and $P^+H_A^-$ is strong enough even for nuclear configurations somewhat distant from the crossing points of the zero-order potential surfaces so that the exact crossing point does not dramatically affect the reaction.

A nearly adiabatic electron-transfer reaction would also explain the discrepancy between the apparent $P^*/P^+H_A^-$ standard free energy gap and the P/P^+ midpoint potential which is observed, particularly at early times and low temperature, when comparing wild-type reaction centers with those from the high-potential mutants [this work and Peloquin et al. (1994)]. If the reaction is adiabatic and the rate is limited by nuclear motion in the system, one would expect the P* population to change in a continuous but not necessarily exponential manner, as the reaction works its way along the potential energy surface away from the region of Frank–Condon overlap with the ground state. In this view, Figures 6 and 7 represent the approximate time dependence of the potential energy of the system as it progresses along the potential surface connecting P* to $P^+H_A^-$. In both R-26 and the double mutant, movement along the potential surface is rate limiting. At early times (picoseconds), when the reaction is in a conformation which is near the crossing point between the zero-order P* and $P^+H_A^-$ potential surfaces, the potential energy change for electron transfer is small for both R-26 and double-mutant reaction centers. Therefore, the large potential differences between the two samples seen on long time scales in the P/P^+ titration measurements are not observed on the picosecond time scale.

One of the hallmarks of a reaction limited by the rate of nuclear conformational change is that the reactants and products do not rapidly achieve thermal equilibrium with the bath on the time scale of the experiment. There are several experimental measurements indicating that thermal equilibration between the vibrational modes coupled to P* formation and those modes in the local environment does not occur completely before charge separation. Middendorf et al. (1991) have suggested an interpretation of photochemical hole-burning experiments relating the width of the zero-phonon hole to the lifetime of P* in which electron transfer precedes vibrational relaxation. Vos et al. (1993) have recently shown that at least two low-energy modes (70 and 15 cm^{-1}) which are strongly coupled to the excited singlet state of P oscillate coherently for picoseconds in a mutant incapable of electron transfer, indicating that they are not well coupled to other modes of the system. If the oscillations observed by Vos et al. (1993) in the transient absorption data are of modes coupled to electron transfer in wild-type reaction centers, then this implies that the reaction coordinate is not well coupled to other vibrational modes and that only a small number of vibrational periods occur on the time scale of electron transfer, consistent with the notion of an adiabatic reaction. As the system takes on more charge-separated character, the coupling with other vibrations and nuclear motions should increase,

presumably through dipolar relaxation of the system.

The obvious problem with the strong coupling model is that calculations based on the ground-state atomic coordinates of the reaction center cofactors and associated molecular orbital calculations have generally yielded coupling energies between P and neighboring chromophores of less than 100 cm^{-1} [e.g., Plato et al. (1988) and Scherer and Fisher (1989)]. It is conceivable that coupling between the cofactors develops after ultrafast changes in the excited singlet state. Changes in the absorption spectrum of P* have been observed on time scales of less than 100 fs, and these include absorption changes in cofactors as far away as the bacteriopheophytins (Vos et al., 1991), possibly indicating changes in the coupling between different cofactors. Further investigations into the evolution of P*, in particular as a function of excitation intensity, are in progress and may help answer some of the questions raised by this work.

ACKNOWLEDGMENT

The authors wish to thank Drs. W. Parson, S. Boxer, D. Holten, D. Gust, and T. Moore for many helpful discussions and P. Horton for preparation of reaction centers.

REFERENCES

Alden, R. G., Cheng, W. D., & Lin, S. H. (1992) *Chem. Phys. Lett. 194*, 318–326.

Allen, J. P., Feher, G., Yeates, T. O., Komiya, H., & Rees, D. C. (1987) *Proc. Natl. Acad. Sci. U.S.A. 84*, 5730–5734.

Chan, C.-K., DiMagno, T. J., Chen, L. X.-Q., Norris, J. R., & Fleming, G. R. (1991) *Proc. Natl. Acad. Sci. U.S.A. 88*, 11202–11206.

Chang, C.-H., El-Kabbani, O., Tiede, D., Norris, J., & Schiffer, M. (1991) *Biochemistry 30*, 5352–5360.

Closs, G. L., & Miller, J. R. (1988) *Science 240*, 440–447.

Deisenhofer, J., Epp, O., Miki, K., Huber, R., & Michel, H. (1984) *J. Mol. Biol. 180*, 385–398.

Du, M., Rosenthal, S. J., Xie, X., DiMagno, T. J., Schmidt, M., Hanson, D. K., Schiffer, M., Norris, J. R., & Fleming, G. R. (1992) *Proc. Natl. Acad. Sci. U.S.A. 89*, 8517–8521.

Feher, G., & Okamura, M. Y. (1978) in *The Photosynthetic Bacteria* (Clayton, R. K., & Sistrom, W. R., Eds.) pp 349–386, Plenum Press, New York.

Feher, G., Allen, J. P., Okamura, M. Y., & Rees, D. C. (1989) *Nature 339*, 111–116.

Goldstein, R. A., Takiff, L., & Boxer, S. G. (1988) *Biochim. Biophys. Acta 934*, 253–263.

Hamm, P., Gray, K. A., Oesterhelt, D., Feick, R., Scheer, H., & Zinth, W. (1993) *Biochim. Biophys. Acta 1142*, 99–105.

Holzapfel, W., Finkele, U., Kaiser, W., Oesterhelt, D., Scheer, H., Stilz, H. U., & Zinth, W. (1989) *Chem. Phys. Lett. 161*, 1–7.

Holzapfel, W., Finkele, U., Kaiser, W., Oesterhelt, D., Scheer, H., Stilz, H. U., & Zinth, W. (1990) *Proc. Natl. Acad. Sci. U.S.A. 87*, 5168–5172.

Horber, J. K. H., Gobel, W., Ogrodnik, A., Michel-Beyerle, M. E., & Cogdell, R. J. (1986) *FEBS Lett. 198*, 273–278.

Kirmaier, C., & Holten, D. (1987) *Photosynth. Res. 13*, 225–260.

Kirmaier, C., & Holten, D. (1988) *FEBS Lett. 239*, 211–218.

Kirmaier, C., & Holten, D. (1990) *Proc. Natl. Acad. Sci. U.S.A. 87*, 3552–3556.

Kirmaier, C., & Holten, D. (1991) *Biochemistry 30*, 609–613.

Kirmaier, C., & Holten, D. (1993) in *The Photosynthetic Reaction Center, Vol. II* (Norris, J. R., Ed.) pp 49–69, Academic Press, San Diego.

Kirmaier, C., Holten, D., & Parson, W. W. (1985) *Biochim. Biophys. Acta 810*, 33–48.

Kirmaier, C., Gaul, D., DeBey, R., Holten, D., & Schenck, C. C. (1991) *Science 251*, 922–927.

Marcus, R. A. (1956) *J. Chem. Phys. 24*, 966–978.

Martin, J.-L., Breton, J., Hoff, A. J., Migus, A., & Antonetti, A. (1986) *Proc. Natl. Acad. Sci. U.S.A. 83*, 957–961.

Middendorf, T. R., Mazzola, L. T., Gaul, D. F., Schenck, C. C., & Boxer, S. G. (1991) *J. Phys. Chem. 95*, 10142–10151.

Morrison, L. E., Schelhorn, J. E., Cotton, T. M., Bering, C. L., & Loach, P. A. (1982) in *Function of Quinones in Energy Conserving Systems* (Trumpower, B. L., Ed.) pp 35–58, Academic Press, New York.

Muller, M. G., Griebenow, K., & Holtzwarth, A. R. (1992) *Chem. Phys. Lett. 199*, 465–469.

Nagarajan, V., Parson, W. W., Davis, D., & Schenck, C. C. (1993) *Biochemistry 32*, 12324–12336.

Ogrodnik, A., Volk, M., Letterer, R., Feick, R., & Michel-Beyerle, M. E. (1988) *Biochim. Biophys. Acta 936*, 361–371.

Parson, W. W. (1991) in *Chlorophylls* (Scheer, H., Ed.) pp 1153–1180, CRC Press, Boca Raton, FL.

Peloquin, J. M., Williams, J. C., Lin, X., Alden, R. G., Taguchi, A. K. W., Allen, J. P., & Woodbury, N. W. (1994) *Biochemistry* (preceding paper in this issue).

Plato, M., Mobius, K., Michel-Beyerle, M. E., Bixon, M., & Jortner, J. (1988) *J. Am. Chem. Soc. 110*, 7279–7285.

Press, W. H., Teukolsky, S. A., Vetterling, W. T., & Flannery, B. P. (1992) in *Numerical Recipes in C, the Art of Scientific Computing*, Cambridge University Press, Cambridge.

Schenck, C. C., Blankenship, R. E., & Parson, W. W. (1982) *Biochim. Biophys. Acta 680*, 44–59.

Scherer, P. O. J., & Fischer, F. (1989) *Chem. Phys. 131*, 115–127.

Sebban, P., & Moya, I. (1983) *Biochim. Biophys. Acta 722*, 436–442.

Taguchi, A. K. W., Stocker, J. W., Alden, R. G., Causgrove, T. P., Peloquin, J. M., Boxer, S. G., & Woodbury, N. W. (1992) *Biochemistry 31*, 10345–10355.

Vos, M. H., Lambry, J. C., Robles, S. J., Youvan, D. C., Breton, J., & Martin, J.-L. (1991) *Proc. Natl. Acad. Sci. U.S.A. 88*, 8885–8889.

Vos, M. H., Lambry, J. C., Robles, S. J., Youvan, D. C., Breton, J., & Martin, J.-L. (1992) *Proc. Natl. Acad. Sci. U.S.A. 89*, 613–617.

Vos, M. H., Rappaport, F., Lambry, J.-C., Breton, J., & Martin, J.-L. (1993) *Nature 363*, 320–325.

Warshel, A. (1980) *Proc. Natl. Acad. Sci. U.S.A. 77*, 3105–3109.

Williams, J. C., Alden, R. G., Murchison, H. A., Peloquin, J. M., Woodbury, N. W., & Allen, J. P. (1992a) *Biochemistry 31*, 11029–11037.

Williams, J. C., Alden, R. G., Coryell, V. H., Lin, X., Murchison, H. A., Peloquin, J. M., Woodbury, N. W., & Allen, J. P. (1992b) in *Research in Photosynthesis* (Murata, N., Ed.), Vol. 1, pp 377–380, Kluwer Academic Publishers, Dordrecht.

Woodbury, N. W. T., & Parson, W. W. (1984) *Biochim. Biophys. Acta 767*, 345–361.